



Originally published as:

Rodríguez-Zuluaga, J., Stolle, C., Park, J. (2017): On the direction of the Poynting flux associated with equatorial plasma depletions as derived from Swarm. - *Geophysical Research Letters*, 44, 12, pp. 5884—5891.

DOI: <http://doi.org/10.1002/2017GL073385>

## RESEARCH LETTER

10.1002/2017GL073385

## Key Points:

- First observational survey of Poynting flux related to equatorial plasma depletions
- Poynting flux and FACs generally organized into interhemispheric flows with seasonal and longitudinal dependency
- Abrupt change in the Poynting flux and FACs direction at about 60°W is likely due to the effect of thermospheric winds and the presence of SAA

## Correspondence to:

J. Rodríguez-Zuluaga,  
 juanzr@gfz-potsdam.de

## Citation:

Rodríguez-Zuluaga, J., C. Stolle, and J. Park (2017), On the direction of the Poynting flux associated with equatorial plasma depletions as derived from *Swarm*, *Geophys. Res. Lett.*, *44*, 5884–5891, doi:10.1002/2017GL073385.




Received 9 MAR 2017

Accepted 15 MAY 2017

Accepted article online 18 MAY 2017

Published online 17 JUN 2017

## On the direction of the Poynting flux associated with equatorial plasma depletions as derived from *Swarm*

J. Rodríguez-Zuluaga<sup>1,2</sup> , C. Stolle<sup>1,2</sup> , and J. Park<sup>3,4</sup> 

<sup>1</sup>GFZ, German Research Centre for Geosciences, Potsdam, Germany, <sup>2</sup>Faculty of Science, University of Potsdam, Potsdam, Germany, <sup>3</sup>Korea Astronomy and Space Science Institute, Daejeon, South Korea, <sup>4</sup>Department of Astronomy and Space Science, University of Science and Technology, Daejeon, South Korea

**Abstract** Magnetic and electric field observations from the European Space Agency *Swarm* mission are used to report the direction of electromagnetic energy flux associated with equatorial plasma depletions. Contrary to expectations, the observations suggest a general interhemispheric Poynting flux rather than concurrent flows at both hemispheres toward or away from the equator. Of high interest is a particular behavior noticed over the region with the largest variation in the magnetic declination. This is a Poynting flux flowing mainly into the southern magnetic hemisphere about between 60°W and 30°E and into the northern magnetic hemisphere between 110°W and 60°W. The abrupt change in the flow direction at 60°W is suggested to be caused by an asymmetry between the hemispheres on the ionospheric conductivity, likely due to the influence of thermospheric winds and the presence of the South Atlantic Anomaly.

### 1. Introduction

Equatorial plasma depletions (EPDs) are macroinstabilities observed as structures of depleted plasma density aligned with the magnetic field in the ionosphere *F* region. They are known to mainly occur at the nighttime geomagnetic equatorial/low latitudes when the ionosphere is unstable due to the steep density gradient in the bottomside *F* region. The physical mechanism responsible for the formation of EPDs was first identified by *Hudson and Kennel* [1975] and their propagation into the topside by *Woodman and La Hoz* [1976]. They were described as the result of both linear and nonlinear growth phases of a plasma boundary instability under the influence of the gravitational field, normally referred as Rayleigh-Taylor or interchange instability [*Ossakow*, 1981; *Hysell*, 2000; *Woodman*, 2009].

Regardless of more than 80 years of efforts understanding the physics behind the occurrence of EPDs and their day-to-day-variability, only a few studies about their electromagnetic features and related Poynting flux from observations have been conducted. This is understood mainly to the lack of simultaneous measurements of both electric and magnetic field at EPDs altitudes of about 150 to 1500 km. However, several satellites have been used to report global observations of EPDs, such as the Atmosphere Explorer [e.g., *McClure et al.*, 1977], Defense Meteorological Satellite Program [e.g., *Huang et al.*, 2001], San Marco D [e.g., *Aggson et al.*, 1992], Communication/Navigation Outage Forecasting System (C/NOFS) [e.g., *Burke et al.*, 2012], and Challenging Minisatellite Payload (CHAMP) [e.g., *Stolle et al.*, 2006] missions.

It is known that EPDs present perturbations in both electric ( $\delta\mathbf{E}$ ) and magnetic ( $\delta\mathbf{B}$ ) fields as a result of currents flowing along and across the depletions. Of importance are magnetic perturbations observed as field fluctuations caused by two types of currents. The first one is attributed to diamagnetic currents (pressure-driven currents) flowing along isodensity contours across the depletions [e.g., *Lühr et al.*, 2003; *Stolle et al.*, 2006]. They are characterized by an enhancement in the magnetic field strength within the EPDs through a balance between the magnetic and plasma pressures. The second type of currents corresponds to field-aligned currents (FACs) flowing within the edges of the depletions [e.g., *Park et al.*, 2009]. They generate transverse magnetic field perturbations as the ones depicted in Figure 1. By assuming electrostatic conditions, these FACs have been traditionally related to the divergence of mainly gravity-driven current at *F* region altitudes [e.g., *Huba et al.*, 2008; *Aveiro and Hysell*, 2012; *Yokoyama and Stolle*, 2016]. A different interpretation stands

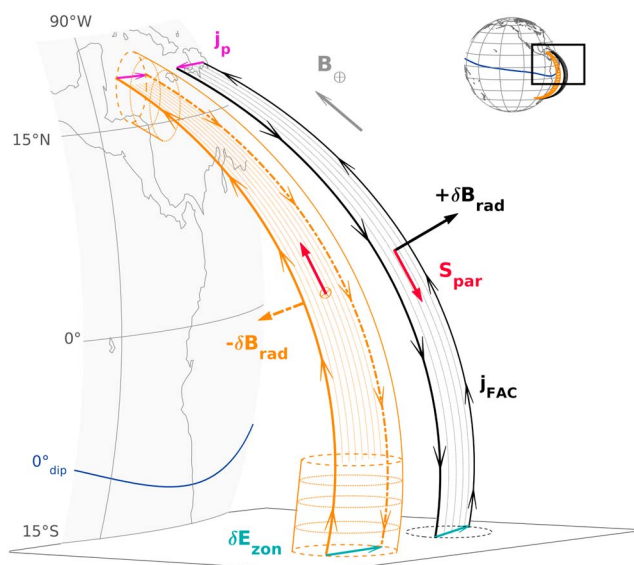


**Figure 1.** Schematic view of two depleted flux tubes with different FACs ( $j_{FAC}$ ) configuration. The FACs-related magnetic signature  $\delta B_{rad}$ , the expected eastward polarization electric field  $\delta E_{zon}$ , the Poynting flux  $S_{par}$  and the polarization currents  $j_p$  are depicted.

in the present study, the direction of the EPDs-related electromagnetic energy flux is reported using simultaneous magnetic and electric field measurements recorded on board the *Swarm* satellites. Two recent studies by *Park et al.* [2016] and *Park et al.* [2017] report observations of the source and Poynting flux direction associated with medium-scale traveling ionospheric disturbances and Alfvén waves at high latitudes, respectively, both by using *Swarm* measurements. So far, there has been no study addressing from observations the Poynting flux related to equatorial plasma depletions.

## 2. Electric and Magnetic Field Data

*Swarm* is the latest mission of the European Space Agency (ESA) to deeply explore the Earth's magnetic field and its temporal evolution. It provides in situ simultaneous high-resolution measurements of magnetic and ion drift (electric fields), plasma density, and both electron and ion temperatures. The constellation consists of three satellites (Alpha, Bravo, and Charlie) placed on near-polar ( $87.5^\circ$  inclination) orbits and flying with a speed of about 7.5 km/s. At the beginning of the mission after its launch on 22 November 2013, the three satellites orbited together at an altitude of about 500 km. Later on 15 April 2014, the satellites reached their final constellation. So far, *Swarm* Bravo orbits with a somewhat higher inclination at an altitude of  $\sim 520$  km. *Swarm* Alpha and Charlie fly side by side with a separation in longitude of  $\sim 1.5^\circ$  at a height of  $\sim 460$  km.

The instruments on board *Swarm* are identical for the three satellites. These are an Absolute Scalar Magnetometer (ASM) and a Vector Field Magnetometer (VSM) recording the total magnetic field at 1 Hz and the three magnetic components at 50 Hz, respectively [Tøffner-Clausen *et al.*, 2016]. A combination of both the ASM and VSM data results in highly accurate vector magnetic field data at a rate of 1 Hz. Two Langmuir probes (LP) provide electron density and electron temperature, and a Thermal Ion Imager (TII) provides ion drift velocity (electric field) and ion temperature [Knudsen *et al.*, 2017]. The LP and TII data appear completely regular at 2 Hz rate. Because both electron density and electric field are not synchronized with the magnetic field data, the first two are decimated to a rate of 1 Hz. An initial release of *Swarm* electric field data has been made available for the period between April and September 2014 for *Swarm*, Alpha, and Bravo. Within this period the data coverage is not continuous and is subjected to large offsets. Then, only data with TII quality flag  $< 30$  are considered, following the recommendation of Knudsen *et al.* [2015]. Additionally, few days available in March 2015 are also included.

Finally, since the magnetic and electric field data are given in North-East-Centre coordinates, the vectors are rotated into the magnetic-field-aligned coordinate system. In this frame the parallel (par) component is

on dynamic electromagnetic characteristics assuming FACs as signatures of Alfvén waves [e.g., Bhattacharyya and Burke, 2000; Pottellette *et al.*, 2007; Lühr *et al.*, 2014]. Despite this discrepancy, it is still assumed in either case that the FACs flow poleward (equatorward) on the external edges of the western (eastern) walls of EPDs, resulting then in a Poynting flux ( $S_{par}$ ) flowing poleward into the *E* region [e.g., Dao *et al.*, 2013]. Nevertheless, the observations reported in this study appear to indicate a new paradigm, consisting of an interhemispherical Poynting flux presumably flowing into the hemisphere with larger ionospheric conductivity.

By using different satellites, investigations about electromagnetic features of EPDs have been conducted using either electric or magnetic field observations [e.g., Aggson *et al.*, 1992; Park *et al.*, 2009; Burke *et al.*, 2012]. In the

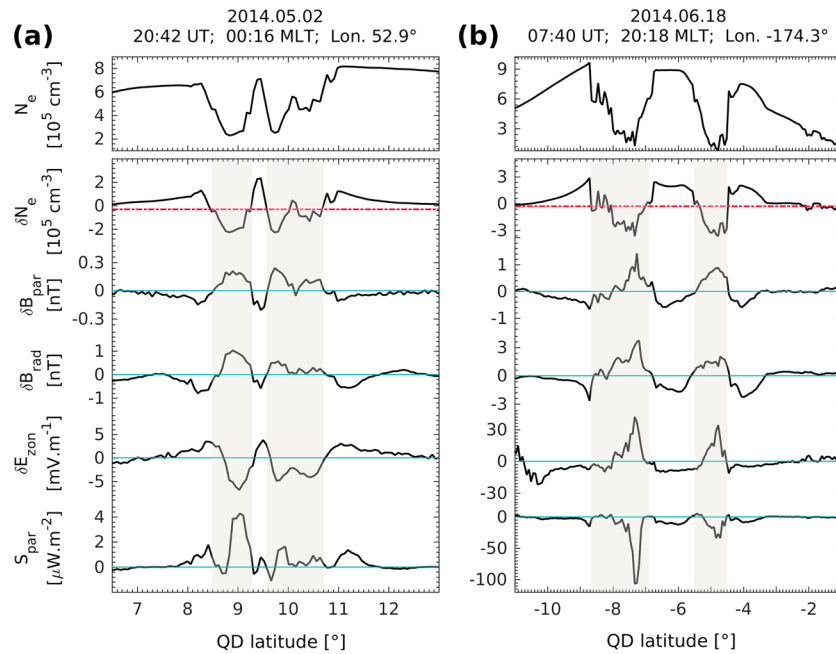


**Figure 2.** Electromagnetic signatures of EPDs as observed by Swarm Alpha. From top to bottom, the electron density ( $N_e$ ) and its residual ( $\delta N_e$ ), the parallel and radial magnetic field components ( $\delta B_{\text{par}}$ ,  $\delta B_{\text{rad}}$ ), the zonal polarization electric field ( $\delta E_{\text{zon}}$ ), and the Poynting flux ( $S_{\text{par}}$ ). (a) Pass over the northern magnetic hemisphere. (b) Pass over the southern magnetic hemisphere. The  $\delta N_e$  threshold ( $-0.3 \times 10^5 \text{ cm}^{-3}$ ) is depicted in red.

aligned with the mean ambient magnetic field, the zonal component (zon) is perpendicular to the magnetic meridian pointing eastward, and the radial (rad) component completes the triad pointing outward to higher L shells.

### 3. EPDs-Related Poynting Flux Estimation

The method to detect EPDs is based on electron density ( $N_e$ ) and magnetic field data, similar to the method implemented by *Park et al.* [2013]. Briefly, the detection is restricted to overpasses of Swarm between  $\pm 30^\circ$  dip latitude and from 18 to 04 magnetic local time (MLT). As a first step, the electron density data are subjected to a high-pass filter in order to withdraw the background values. The resulting residual  $\delta N_e$  is considered if almost continuous values  $\leq -0.3 \times 10^5 \text{ cm}^{-3}$  are present (see Figures 2a and 2b, second panel). Subsequently, in order to guarantee that such depletions correspond to EPDs, the plasma density must be correlated with the magnetic field strength and transverse components within the depletion. Hereof, the magnetic field contributions from the core, lithosphere, and magnetosphere are subtracted from the magnetic field measurements by using the geomagnetic field model CHAOS6 [*Finlay et al.*, 2016]. The resulting values are residuals assumed to be of ionospheric origin ( $\delta B_{\text{par}}$ ,  $\delta B_{\text{zon}}$ , and  $\delta B_{\text{rad}}$ ).

Accordingly, the EPD events considered in this study are those that present linear correlation between  $\delta N_e$  and both the  $\delta B_{\text{par}}$  and  $\delta B_{\text{rad}}$  with correlation coefficients ( $cc$ )  $\leq -0.6$  and  $|cc| \geq 0.6$ , respectively. These magnetic perturbations are attributed to the diamagnetic and field-aligned currents effect.

With respect to the electric field, the background values are removed using a high-pass filter, resulting then in the components  $\delta E_{\text{zon}}$  and  $\delta E_{\text{rad}}$ , corresponding to the electric field fluctuation across the depletion and which direction is relative to the background electric field.

The Poynting flux derived is the one parallel to the main magnetic field,

$$S_{\text{par}} = \frac{\delta \mathbf{E}_{\perp} \times \delta \mathbf{B}_{\perp}}{\mu_0} = \frac{(\delta E_{\text{rad}} + \delta E_{\text{zon}}) \times (\delta B_{\text{rad}} + \delta B_{\text{zon}})}{\mu_0}. \quad (1)$$

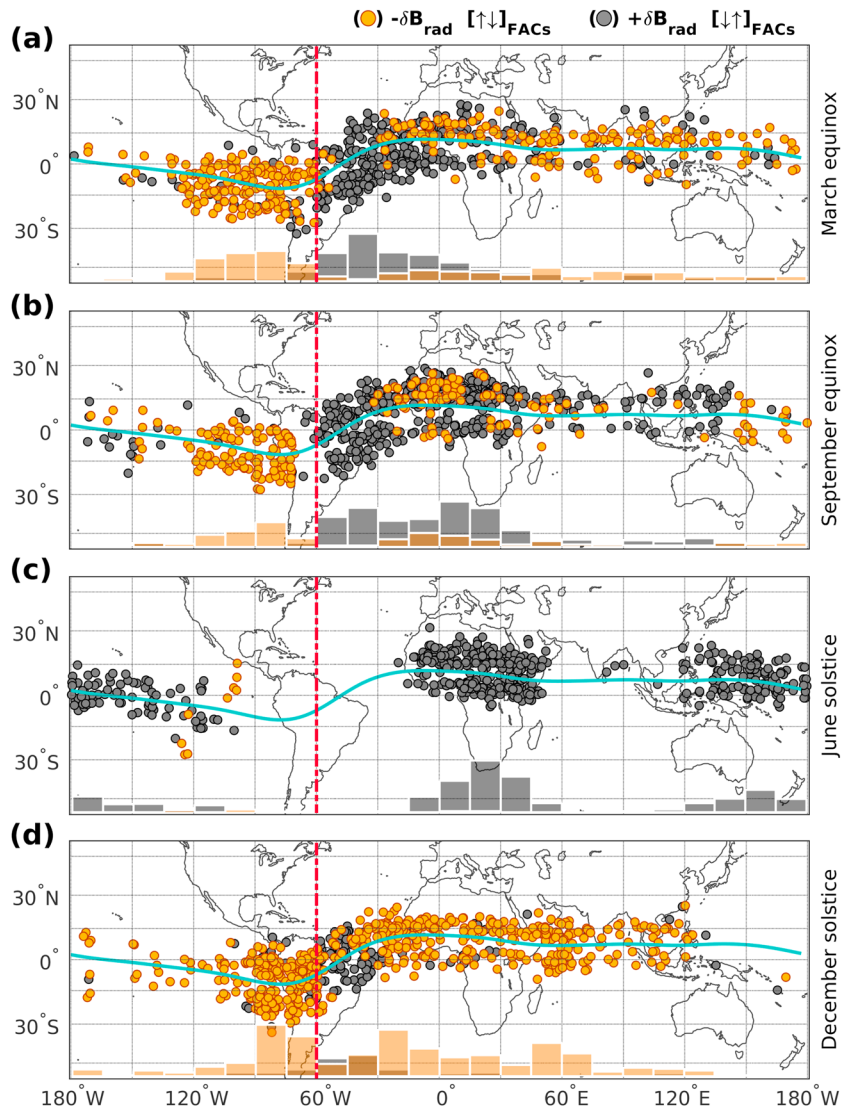


**Figure 3.** EPD events displayed by season and set by the polarization of the FACs-related magnetic signature  $\delta\mathbf{B}_{\text{rad}}$  (dots). (a) March equinox, (b) September equinox, (c) June solstice, and (d) December solstice. The sudden change in the FACs direction is indicated by the dashed red line. The longitudinal variation of the occurrence of EPD events is qualitatively shown by histograms at the bottom of each panel.

To compute the  $\mathbf{S}_{\text{par}}$ , the electric and magnetic field components ( $\delta\mathbf{E}_{\text{zon}}$ ,  $\delta\mathbf{B}_{\text{rad}}$  and  $\delta\mathbf{E}_{\text{rad}}$ ,  $\delta\mathbf{B}_{\text{zon}}$ ) must be well correlated ( $|\text{cc}| \geq 0.6$ ). In order to strengthen the conclusions of this study, and since the set of electric field data is limited and subjected to offsets, the  $\mathbf{S}_{\text{par}}$  is computed only with one pair of  $\delta\mathbf{E}_{\perp}$  and  $\delta\mathbf{B}_{\perp}$  if the other pair of components is not well correlated, otherwise, both pairs are used in the computation. This approach is acceptable since the aim of this study is the analysis of the  $\mathbf{S}_{\text{par}}$  direction, not its magnitude. Additionally, to avoid nongeophysical signals mainly from the electric field data, a cross check is done to guarantee agreement between both the electric and magnetic field data. This is done by inferring the tilt of the depletion separately with  $\delta\mathbf{E}_{\perp}$  and  $\delta\mathbf{B}_{\perp}$ , which must result in agreement to be considered. The EPDs tilt can be inferred via the sign of the linear correlation between the two components of either  $\delta\mathbf{E}_{\perp}$  or  $\delta\mathbf{B}_{\perp}$ . This cross check is carried out only for EPDs that present well correlation between the two pairs of  $\delta\mathbf{E}_{\perp}$  and  $\delta\mathbf{B}_{\perp}$  components. Finally, to deduce the  $\mathbf{S}_{\text{par}}$  direction, the mean is calculated over the EPD interval determined by the threshold in  $\delta N_e$  and highlighted with gray bands as shown in Figure 2. Thus, a positive value corresponds to a  $\mathbf{S}_{\text{par}}$  flowing northward.



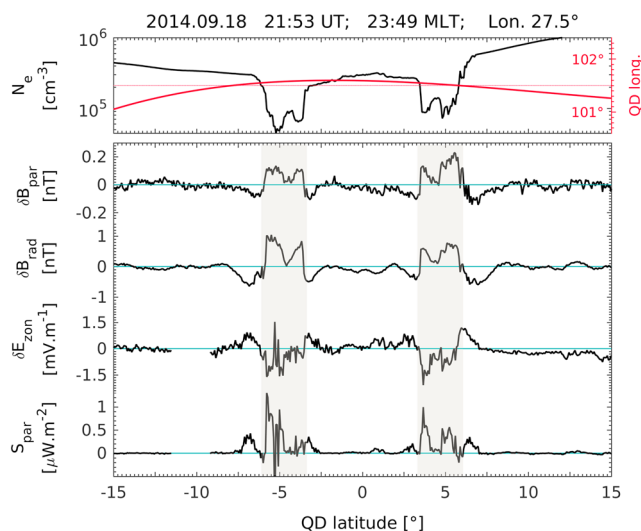


**Figure 4.** Pass of Swarm Alpha. (from top to bottom) The electron density ( $N_e$ ) and the path of the satellite in quasi-dipole longitude (QD longitude), the parallel and radial magnetic field components ( $\delta B_{\text{par}}$ ,  $\delta B_{\text{rad}}$ ), the zonal polarization electric field ( $\delta E_{\text{zon}}$ ) and the Poynting flux ( $S_{\text{par}}$ ).

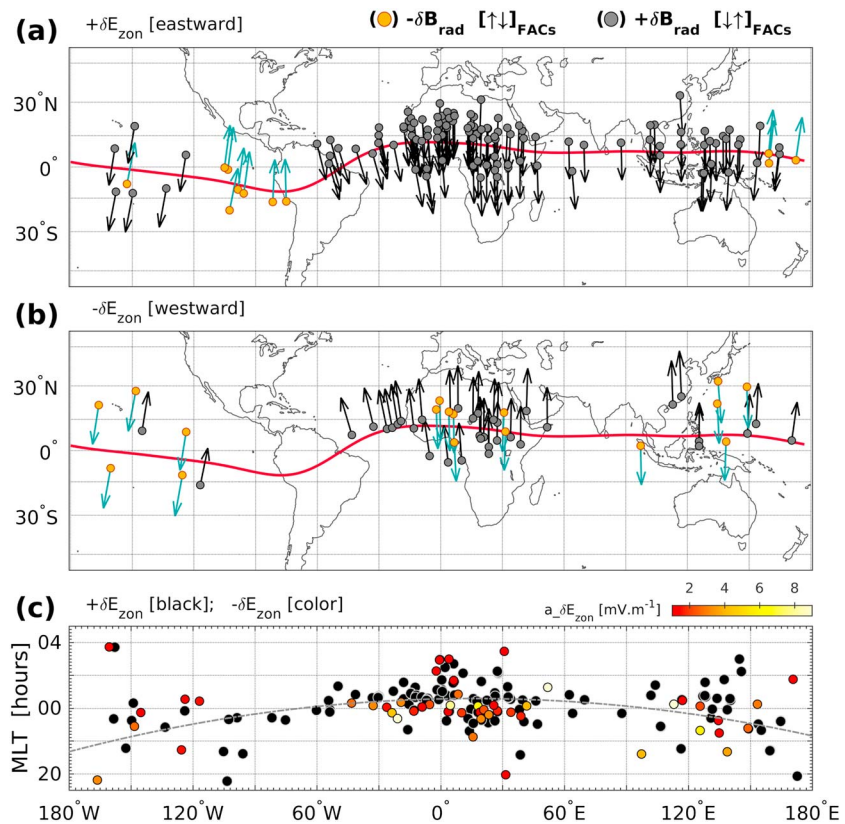
#### 4. Observations and Discussion

Figure 2 shows two passes of Swarm over the northern and southern magnetic hemispheres. They both present EPD events with clear electromagnetic signatures. Of great interest is the westward electric field  $\delta E_{\text{zon}}$  registered within the depletions in Figure 2a. This westward  $\delta E_{\text{zon}}$  measured across EPDs is associated with downward plasma convection and is commonly observed on satellites, such as the San Marco D [e.g., *Laakso et al.*, 1994], AE-E [e.g., *Singh et al.*, 1999], DE-2 [e.g., *Palmroth et al.*, 2000], and C/NOFS [e.g., *Haaser et al.*, 2012; *Burke et al.*, 2012], and by radars [e.g., *Rao et al.*, 1997; *Fukao et al.*, 2004; *Saito et al.*, 2008; *Patra et al.*, 2014]. By definition, the zonal polarization electric field within a depletion is expected to be eastward since it is built to keep the continuity of the gravity-driven current  $\mathbf{j} = nM(\mathbf{g} \times \mathbf{B})/B^2$ , being  $n$  and  $M$  the local

plasma density and the mass of its constituent ion species, respectively. As suggested by *Laakso et al.* [1994], downward plasma convection associated with westward  $\delta E_{\text{zon}}$  across depletions can occur likely by either a change in the background electric field from eastward to westward or by responding to slow or negative vertical neutral winds when the ion-neutral collision frequency is fairly large. Based on the altitude of about 500 km at which Swarm records their measurements, it seems improbable to find large ion-neutral collision frequencies at heights above the  $F$  peak. A different explanation based on measurements gathered by C/NOFS is suggested by *Burke et al.* [2012]. The authors propose that such kind of observations corresponds to the local part of the perturbed interface that experiences the downward drift due to the westward  $\delta E_{\text{zon}}$  (see their Figure 12), and that in turn, they should not be considered as EPDs. However, not having a complete picture of the depletion makes the interpretation challenging, since they can also be attributed to fossil bubbles as suggested by different authors [e.g. *Aggson et al.*, 1992; *Krall et al.*, 2010, and references therein]. Standing on the observations presented in this study, it seems that the change of sign of the background electric field is the most likely cause of westward polarization electric field within EPDs, as it will be shown later in this section.

The direction of the FACs flowing along the walls of EPDs is determined solely by the direction of  $\delta B_{\text{rad}}$  (see Figure 1). In Figure 3 the detected EPDs are characterized by the direction of FACs and presented for the two equinoxes and solstices. The color of the dots is related to the direction of the FACs as the ones depicted in Figure 1. In the bottom of each of the four panels, a histogram shows the quantity of EPD events. Each bin corresponds to 15° in geographic longitude, and the color (yellow and grey) is in accordance with the color of the dots. The histograms do not present explicitly the number of EPDs, they are scaled for each panel and are shown to qualitatively highlight the longitudinal variation of the occurrence of EPDs. The data used correspond to measurements of the three Swarm satellites during 2014 and 2015. In general, the EPDs are well distributed along the globe and suggest a seasonal-spatial variation in agreement with previous climatological studies [e.g., *Xiong et al.*, 2010, and references therein]. An interesting observation is the general flow of FACs from local summer to winter during both June and December solstices (see Figures 3c and 3d). Even more exciting is the sudden change in the FACs direction at about 60°W during March and September equinoxes, and December solstice (see Figures 3a, 3b, and 3d, vertical red line). This interhemispheric flow of FACs differs from the general assumption of FACs flowing poleward on western walls and equatorward on eastern walls of EPDs.

It is proposed that a likely cause for such interhemispheric flow could be a dissimilarity in the Pedersen conductivity between both magnetic hemispheres. As it is known, the electric currents flow through all possible paths but more current will flow through the lower resistance path. Thus, in a general way, it might



**Figure 5.** EPDs as observed by the polarization of the FACs-related magnetic signature  $\delta\mathbf{B}_{\text{rad}}$  (dots) and the direction of the Poynting flux  $\mathbf{S}_{\text{par}}$  (arrows). Set by (a) eastward polarization electric field  $\delta\mathbf{E}_{\text{zon}}$  and (b) westward polarization electric field  $\delta\mathbf{E}_{\text{zon}}$ . (c) EPD events in Figures 5a and 5b as a function of magnetic local time and longitude.

be expected, for instance, that FACs in the vicinities of the South Atlantic Anomaly where a larger Pedersen conductivity is present, tend to flow mainly into the southern magnetic hemisphere. Furthermore, summer-to-winter transequatorial winds in the thermosphere are expected to enhance conductivity in the winter hemisphere [Maruyama, 1988, Figures 7d and 8d] in agreement with the observations presented during both June and December solstices (see Figures 3c and 3d). During March and September equinoxes (Figures 3a and 3b), the sudden change in the FACs direction at about 60°W, and in turn, of the Poynting flux direction is of great interest. This could be interpreted as due to the contribution of zonal winds to the field-aligned wind component in the presence of large magnetic declination angles. Generally, zonal winds in the nighttime thermosphere blow eastward, irrespective of season [e.g., Drob et al., 2015, Figure 4]. When combined with the eastward tilt of the geomagnetic field between about 180°W and 70°W, the eastward wind in the geographic frame can contribute to field-aligned plasma transport from the Southern Hemisphere to the Northern Hemisphere. According to Maruyama [1988], the northward transport should lead to enhanced ionospheric conductivity in the northern magnetic hemisphere. Besides, when combined with the westward tilt of the geomagnetic field between about 70°W and 20°W, the eastward wind can contribute to the already larger conductivity in the southern magnetic hemisphere by increasing the plasma transport from the Northern Hemisphere to the Southern Hemisphere.

In order to support the fact that the direction of the FACs is different than expected, Figure 4 shows an example of Swarm Alpha passing across two depletions  $\pm 5^\circ$  away from the dip Equator. In the top of the figure (in red) the path of the satellite is depicted in quasi-dipole coordinates together with the electron density. It is noticed that both depletions are roughly in the same magnetic meridian, suggesting the possibility of being the same depleted flux tube. When looking at the  $\delta\mathbf{B}_{\text{rad}}$  (third panel) both depletions present positive fluctuations, implying then an interhemispheric FACs flow. Likewise, the  $\mathbf{S}_{\text{par}}$  in the bottom of the figure describes also an interhemispheric Poynting flux. Because of the relevance of these findings, a more detailed analysis on the climatology of FACs is warranted and will be addressed in another study.

In Figure 5 the direction of the Poynting flux is shown for some selected EPDs based on the availability of electric field data. The EPDs are displayed in two panels depending on the  $\delta E_{z\text{on}}$  polarization, eastward in Figure 5a and westward in Figure 5b. The direction of the FACs is also depicted with yellow and gray dots as in Figure 3. Since most of the  $S_{\text{par}}$  observations reported in this study are centered around June, a larger number of EPDs over Africa is noticed. Of the total number of events with  $S_{\text{par}}$  computed, 71% correspond to EPDs with eastward  $\delta E_{z\text{on}}$  and 29% with westward  $\delta E_{z\text{on}}$ . In Figure 5c, both the EPDs in Figures 5a and 5b are displayed as a function of longitude and magnetic local time. The EPDs with eastward and westward  $\delta E_{z\text{on}}$  are in black and color, respectively. In general, it is noticed that the EPDs between about 60°W to 60°E mainly occur later in the evening compared to the EPDs in other longitudes. This characteristic was also noticed by *Stolle et al.* [2008] using data from the CHAMP and ROCSAT-1 satellites. In the study, the authors report high agreement between the vertical plasma drift and the occurrence rate of depletions. In their Figure 6, it is shown that during June solstice the pre-reversal enhancement peak velocity occurs later in the evening between about 45°W and 45°E, in accordance with other studies [e.g., *Fejer et al.*, 2008, Figure 4]. In particular, it is noticed that EPDs with westward  $\delta E_{z\text{on}}$  occur generally after 22:00 MLT, with the premidnight EPDs presenting larger amplitudes than the few postmidnight ones. However, one must be aware of the bias of this distribution by the disrupted and limited set of data. In contrast, westward  $\delta E_{z\text{on}}$  across depletions was also reported by *Haaser et al.* [2012] using measurements gathered by C/NOFS. The authors account for depletions of this kind to occur throughout the night, and in some cases to have the same occurrence rate than depletions with eastward  $\delta E_{z\text{on}}$  (see their Figure 6). Therefore, it can be said that depletions with westward  $\delta E_{z\text{on}}$  are commonly observed throughout the night with a higher occurrence rate later in the evening (after ~22:00 LT) when the ambient electric field has become westward.

## 5. Summary and Conclusions

This study reports observations of the Poynting flux direction associated with equatorial plasma depletions as derived from the Swarm constellation. By using simultaneous measurements of electric and magnetic fields, the EPDs-related Poynting flux is estimated for a limited set of data. Furthermore, the direction of the related FACs is derived by their associated magnetic field perturbations. The main findings and conclusions could be summarized as follows.

1. The EPDs-related FACs present interhemispheric flows rather than poleward and equatorward flows at each hemisphere on the western and eastern EPD walls, respectively.
2. In turn, a general interhemispherical Poynting flux is deduced to be mainly from summer to winter during solstice. During equinox, a preference for northward Poynting flux from about 110°W to 60°W (positive magnetic declination) and southward from 60°W to 30°E (negative magnetic declination) is observed.
3. The sudden change in the flow of both Poynting flux and FACs at about 60°W can be interpreted as the influence of thermospheric zonal winds in the presence of large magnetic declination angles. This occurs by affecting the field-aligned transport of plasma, which in consequence yields to a hemispheric asymmetry of the ionospheric conductivity. Furthermore, the South Atlantic Anomaly may also enhance ionospheric conductivity in the Southern Hemisphere to the east of 60°W.
4. Among the total number of EPDs with Poynting flux reported, 71% present eastward polarization electric field  $\delta E_{z\text{on}}$  and 29% westward  $\delta E_{z\text{on}}$  across the depletions. To support these observations, a further analysis should be carried out when more calibrated electric field data are available from the Swarm mission.

Certainly, an extended data set is warranted in order to investigate further spatial and temporal variations of the EPDs-related electromagnetic features. Moreover, comparison with simulations and ground-based measurements are essential for a better understanding of individual features of EPDs, such as the tilt, that is expected to influence the magnitude of magnetic deflections perpendicular to the ambient magnetic field.

## References

- Aggson, T. L., N. C. Maynard, W. B. Hanson, and J. L. Saba (1992), Electric field observations of equatorial bubbles, *J. Geophys. Res.*, *97*(A3), 2997–3009.
- Aveiro, H. C., and D. L. Hysell (2012), Implications of the equipotential field line approximation for equatorial spread *F* analysis, *Geophys. Res. Lett.*, *39*, L11106, doi:10.1029/2012GL051971.
- Bhattacharyya, A., and W. J. Burke (2000), A transmission line analogy for the development of equatorial ionospheric bubbles, *J. Geophys. Res.*, *105*(A11), 24,941–24,950.
- Burke, W. J., L. C. Gentile, S. R. Shomo, P. A. Roddy, and R. F. Pfaff (2012), Images of bottomside irregularities observed at topside altitudes, *J. Geophys. Res.*, *117*, A03332, doi:10.1029/2011JA017169.

### Acknowledgments

The authors appreciate valuable discussions with J. “Koki” Chau and the Swarm EFi team at the University of Calgary. The authors are also grateful to the Reviewers for the precise and constructive comments. The European Space Agency (ESA) is acknowledged for providing the Swarm data, which are accessible via <https://earth.esa.int/web/guest/swarm/data-access>. J. Rodríguez-Zuluaga is supported by the Special Priority Programme (SPP) 1788 “DynamicEarth” of the German Research Foundation (DFG).



- Dao, E., C. E. Seyler, and M. C. Kelley (2013), Three-dimensional modeling of the electromagnetic characteristics of equatorial plasma depletions, *J. Geophys. Res. Space Physics*, *118*, 3505–3514, doi:10.1002/jgra.50216.
- Drob, D. P., et al. (2015), An update to the Horizontal Wind Model (HWM): The quiet time thermosphere, *Earth Space Sci.*, *2*(7), 301–319.
- Fejer, B. G., J. W. Jensen, and S.-Y. Su (2008), Quiet time equatorial *F* region vertical plasma drift model derived from ROCSAT-1 observations, *J. Geophys. Res.*, *113*, A05304, doi:10.1029/2007JA012801.
- Finlay, C. C., N. Olsen, S. Kotsiaros, N. Gillet, and L. Tøffner-Clausen (2016), Recent geomagnetic secular variation from Swarm and ground observatories as estimated in the CHAOS-6 geomagnetic field model, *Earth Planets Space*, *68*(1), 1–18.
- Fukao, S., Y. Ozawa, T. Yokoyama, M. Yamamoto, and R. T. Tsunoda (2004), First observations of the spatial structure of *F* region 3-m-scale field-aligned irregularities with the Equatorial Atmosphere Radar in Indonesia, *J. Geophys. Res.*, *109*, A02304, doi:10.1029/2003JA010096.
- Haaser, R. A., G. D. Earle, R. A. Heelis, J. Klenzing, R. Stoneback, W. R. Coley, and A. G. Burrell (2012), Characteristics of low-latitude ionospheric depletions and enhancements during solar minimum, *J. Geophys. Res. Space Physics*, *117*, A10305, doi:10.1029/2012JA017814.
- Huang, C. Y., W. J. Burke, J. S. Machuzak, L. C. Gentile, and P. J. Sultan (2001), DMSP observations of equatorial plasma bubbles in the topside ionosphere near solar maximum, *J. Geophys. Res.*, *106*(A5), 8131–8142.
- Huba, J. D., G. Joyce, and J. Krall (2008), Three-dimensional equatorial spread *F* modeling, *Geophys. Res. Lett.*, *35*, L10102, doi:10.1029/2008GL033509.
- Hudson, M. K., and C. F. Kennel (1975), Linear theory of equatorial spread *F*, *J. Geophys. Res.*, *80*(34), 4581–4590.
- Hysell, D. L. (2000), An overview and synthesis of plasma irregularities in equatorial spread *F*, *J. Atmos. Sol. Terr. Phys.*, *62*(12), 1037–1056.
- Knudsen, D., J. Burchill, S. Buchert, I. Coco, L. Tøffner-Clausen, and P. E. Holmdahl Olsen, (2015), Swarm preliminary plasma dataset user note, Tech. Note SWAM-GSEG-EOPG-TN-15-0003, pp. 2-12, European Space Agency (ESA), Frascati, Italy.
- Knudsen, D. J., J. K. Burchill, S. C. Buchert, A. I. Eriksson, R. Gill, J.-E. Wahlund, L. Åhlen, M. Smith, and B. Moffat (2017), Thermal ion imagers and Langmuir probes in the Swarm electric field instruments, *J. Geophys. Res. Space Physics*, *122*, 2655–2673, doi:10.1002/2016JA022571.
- Krall, J., J. D. Huba, S. L. Ossakow, and G. Joyce (2010), Why do equatorial ionospheric bubbles stop rising?, *Geophys. Res. Lett.*, *37*, L09105, doi:10.1029/2010GL04312.
- Laakso, H., T. L. Aggson, R. F. Pfaff, and W. B. Hanson (1994), Downdrafting plasma flow in equatorial bubbles, *J. Geophys. Res.*, *99*(A6), 11,507–11,515.
- Lühr, H., M. Rother, S. Maus, W. Mai, and D. Cooke (2003), The diamagnetic effect of the equatorial Appleton anomaly: Its characteristics and impact on geomagnetic field modeling, *Geophys. Res. Lett.*, *30*(17), 1906, doi:10.1029/2003GL017407.
- Lühr, H., J. Park, C. Xiong, and J. Rauberg (2014), Alfvén wave characteristics of equatorial plasma irregularities in the ionosphere derived from CHAMP observations, *Front. Phys.*, *2*, 47.
- Maruyama, T. (1988), A diagnostic model for equatorial Spread *F*: 1. Model description and application to electric field and neutral wind effects, *J. Geophys. Res.*, *93*(A12), 14611–14622.
- McClure, J. P., W. B. Hanson, and J. H. Hoffman (1977), Plasma bubbles and irregularities in the equatorial ionosphere, *J. Geophys. Res.*, *82*(19), 2650–2656.
- Ossakow, S. L. (1981), Spread-*F* theories: A review, *J. Atmos. Terr. Phys.*, *43*(5-6), 437–452.
- Palmroth, M., H. Laakso, B. G. Fejer, and R. F. Pfaff (2000), DE-2 observations of morningside and eveningside plasma density depletions in the equatorial ionosphere, *J. Geophys. Res.*, *105*(A8), 18,429–18,442.
- Park, J., H. Lühr, C. Stolle, M. Rother, K. W. Min, and I. Michaelis (2009), The characteristics of field-aligned currents associated with equatorial plasma bubbles as observed by the CHAMP satellite, *Ann. Geophys.*, *27*, 2685–2697.
- Park, J., M. Noja, C. Stolle, and H. Lühr (2013), The Ionospheric Bubble Index deduced from magnetic field and plasma observations onboard Swarm, *Earth Planets Space*, *65*(11), 1333–1344.
- Park, J., H. Lühr, C. Stolle, J. Rodríguez-Zuluaga, D. J. Knudsen, J. K. Burchill, and Y. S. Kwak (2016), Statistical survey of nighttime midlatitude magnetic fluctuations: Their source location and Poynting flux as derived from the Swarm constellation, *J. Geophys. Res. Space Physics*, *121*, 11,235–11,248, doi:10.1002/2016JA023408.
- Park, J., H. Lühr, D. J. Knudsen, J. K. Burchill, and Y. S. Kwak (2017), Alfvén waves in the auroral region, their Poynting flux, and reflection coefficient as estimated from Swarm observations, *J. Geophys. Res. Space Physics*, *122*, 2345–2360, doi:10.1002/2016JA023527.
- Patra, A. K., P. Srinivasulu, P. P. Chaitanya, M. D. Rao, and A. Jayaraman (2014), First results on low-latitude *E* and *F* region irregularities obtained using the Gadanki ionospheric radar interferometer, *J. Geophys. Res. Space Physics*, *119*, 10,276–10,293, doi:10.1002/2014JA020604.
- Pottelette, R., M. Malingre, J. J. Berthelier, E. Seran, and M. Parrot (2007), Filamentary Alfvénic structures excited at the edges of equatorial plasma bubbles, *Ann. Geophys.*, *25*(10), 2159–2165.
- Rao, P. B., A. K. Patra, T. C. Sarma, B. K. Murthy, K. S. Rao, and S. S. Hari (1997), Radar observations of updrafting and downdrafting plasma depletions associated with the equatorial spread *F*, *Radio Sci.*, *32*(3), 1215–1227.
- Saito, S., S. Fukao, M. Yamamoto, Y. Otsuka, and T. Maruyama (2008), Decay of 3-m-scale ionospheric irregularities associated with a plasma bubble observed with the Equatorial Atmosphere Radar, *J. Geophys. Res.*, *113*, A11318, doi:10.1029/2008JA013118.
- Singh, S., F. S. Johnson, and R. A. Heelis (1999), Singular plasma disturbances in the low-latitude *F* region, *J. Geophys. Res.*, *104*(A3), 4337–4350.
- Stolle, C., H. Lühr, M. Rother, and G. Balasis (2006), Magnetic signatures of equatorial spread *F* as observed by the CHAMP satellite, *J. Geophys. Res.*, *111*, A02304, doi:10.1029/2005JA011184.
- Stolle, C., H. Lühr, and B. G. Fejer (2008), Relation between the occurrence rate of ESF and the vertical plasma drift velocity at sunset derived from global observations, *Ann. Geophys.*, *26*(12), 3979–3988.
- Tøffner-Clausen, L., V. Lesur, N. Olsen, and C. C. Finlay (2016), In-flight scalar calibration and characterisation of the Swarm magnetometry package, *Earth Planets Space*, *68*(1), 129.
- Woodman, R. F., and C. La Hoz (1976), Radar observations of *F* region equatorial irregularities, *J. Geophys. Res.*, *81*(31), 5447–5466.
- Woodman, R. F. (2009), Spread *F*—An old equatorial aeronomy problem finally resolved?, *Ann. Geophys.*, *27*(5), 1915–1934.
- Xiong, C., J. Park, H. Lühr, C. Stolle, and S. Y. Ma (2010), Comparing plasma bubble occurrence rates at CHAMP and GRACE altitudes during high and low solar activity, *Ann. Geophys.*, *28*(9), 1647–1658.
- Yokoyama, T., and C. Stolle (2016), Low and midlatitude ionospheric plasma density irregularities and their effects on geomagnetic field, *Space Sci. Rev.*, *27*(5), 1821–1830.